Supplementary Information (SI) for Journal of Materials Chemistry C.

Hysteresis-Encoded Thermometry in the Cryogenic Regime Using Dy-Single-Molecule Magnet

Shraoshee Shome[a], Sanjit Konar*[a]

[a] Shraoshee Shome, Prof. Sanjit Konar
Molecular Magnetism Lab, Department of Chemistry
Indian Institute of Science Education and Research, Bhopal
Bhopal Bypass Road, Bhauri, Madhya Pradesh, India- 462066
E-mail: skonar@iiserb.ac.ins

Contents:

S1. Experimental Section and Characterisations

Materials

All the reagents are commercially available and used without further purification. All chemicals are purchased from Sigma Aldrich Pvt. Ltd. Solvents were used as received.

Physical Measurements

IR spectra were recorded with a Spectrum two spectrometer (PerkinElmer Inc.) in attenuated-total-reflectance (ATR) mode under ambient conditions. Spectra were recorded at 4 cm^{-1} resolution with a wavelength range of 4000-400 cm^{-1}. Elemental analyses (CHNS) were performed at the Elementar Micro Vario Cube elemental analyzer.

Powder XRD was carried out in the PANalytical EMPYREAN instrument using Cu Kα radiation. PerkinElmer TGA 4000 thermogravimetric analyzer was used for the thermodynamic analysis of all the samples with an alumina sample holder and an N_2 flow of 10 mL per minute. The analysis was carried out between 30 °C to 600 °C at a heating rate of 5 °C per minute.

Magnetic Measurements

Magnetic measurements were performed using a Quantum Design SQUID-VSM (MPMS) magnetometer. The hysteresis measurements were performed in a -3.5 to 3.5 T field range with varying scan rates of 100/200/300 Oe s^{-1} in a 2-8 K temperature range.

Magnetothermometry using hysteresis

Equations S1 and S2 are used to calculate the relative thermal sensitivity (S_r), and temperature uncertainty (δT), respectively. Here Δ is the thermometry parameter (remanent magnetisation/saturation magnetisation/loop area). δΔ/Δ represents the relative uncertainty on each of the thermometry parameters.

$$S_r = \frac{1}{\Delta}\left(\frac{\delta\Delta}{\delta T}\right) \quad \text{.....Equation S1}$$

$$\delta T = \frac{1}{S_r}\left(\frac{\delta\Delta}{\Delta}\right) \quad \text{.....Equation S2}$$

The Δ *vs* T plots were fitted considering a phenomenological model using the Boltzmann sigmoidal equation S3 in Origin software.

$$\Delta = A_2 + \frac{A_1 - A_2}{1+\exp\left(\frac{T-T_o}{dT}\right)} \quad \text{.....Equation S3}$$

Where A_1 and A_2 are the values of thermometry parameters at low and high temperatures, respectively, T_o is the midpoint temperature where the transition occurs, and dT is the width of the transition (i.e., the steepness of the Δ vs T curve).

To assess reproducibility, each hysteresis measurement at a given scan rate was repeated three times under identical conditions, and the standard deviation of the resulting values was used to estimate δΔ/Δ. The corresponding error bars are shown as temperature uncertainty δT.

Syntheses of Complexes

Synthesis of $[Dy_2(BBPEN)_2Cl]$ (Complex 1)

The ligand H_2BBPEN was synthesized following the reported procedure.[1]

$[Dy_2(BBPEN)_2Cl]$ was prepared following the reported procedure.[2] To a solution of $DyCl_3{\cdot}6H_2O$ (37 mg, 0.1 mmol) and H_2BBPEN (46 mg, 0.1 mmol) in Methanol (5 mL), triethylamine (~30 μL, 0.2 mmol) was added dropwise. After stirring for 5 min, the resulting mixture was immediately filtered, and the filtrate was left to stand at room temperature for slow evaporation. The product was obtained as a colorless block crystal after 1 day (Yield~77% based on Dy).

Elem anal ($C_{28}H_{28}N_4O_2DyCl$): Calcd C, 51.70; H, 4.34; N, 8.61. Found: C, 51.71; H, 4.28; N, 8.58.

Synthesis of $[Dy(L^{N6}_{phen})(Ph_3SiO)_2](PF_6)$ (Complex 2)

The complex 2 was synthesised following the reported procedure.[3] A mixture of 1,10-phenanthroline-2,9-dicarbaldehyde (0.20 mmol, 0.047 g), triethylenetetramine (0.20 mmol, 0.030 g), and $DyCl_3{\cdot}6H_2O$ (0.20 mmol, 0.075 g) was dissolved in 15 mL of methanol, affording a clear orange solution. The reaction mixture was heated under reflux for 24 h, after which the solvent was evaporated under reduced pressure, leaving behind an orange-yellow oily residue. This residue was treated with a dichloromethane solution (15 mL) of Ph_3SiOH (0.80 mmol, 0.222 g) and Et_3N (0.80 mmol, 0.112 mL). Subsequently, an aqueous solution of NH_4PF_6 (0.20 mmol, 0.032 g, 15 mL) was added, resulting in the formation of a biphasic system. The mixture was refluxed for an additional hour, and the organic phase (CH_2Cl_2) was separated using a separatory funnel, then filtered to obtain a clear yellow solution. Slow diffusion of n-pentane into this solution over 2–3 days yielded pale yellow plate-shaped crystals suitable for single-crystal X-ray diffraction. The crystals were collected by filtration, washed with CH_2Cl_2 (2 × 2 mL), and dried in air to give the product (Yield 35 % based on Dy).

Elem anal ($C_{56}H_{52}DyF_6N_6O_2PSi_2$): Calculated C, 55.83; H, 4.35; N, 6.98. Found: C, 55.70; H, 4.22; N, 6.95.

S2. IR spectroscopy

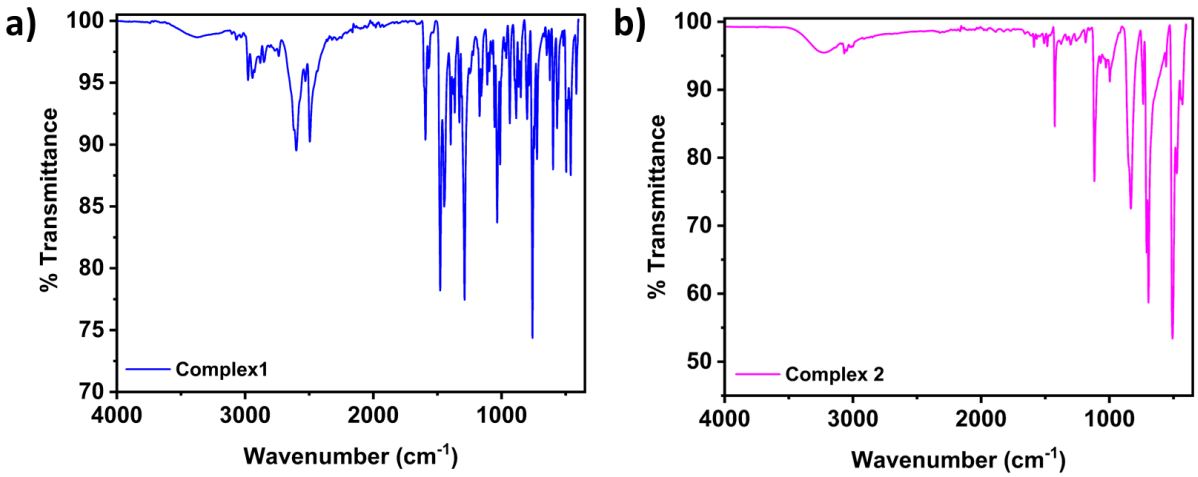

Figure S1: IR spectrum of a) complex 1and b) complex 2.

S3. Powder X-ray diffraction analysis

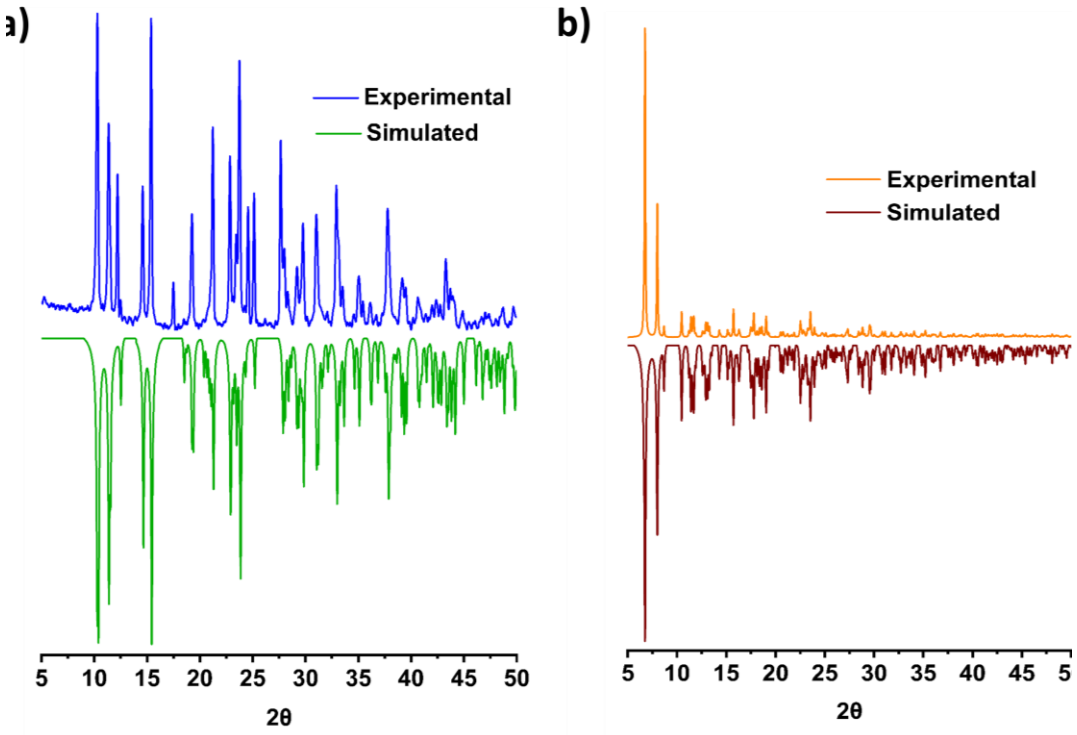

Figure S2: Powder X-ray diffraction pattern of a) complex 1 and b) complex 2.

S6. Thermogravimetric analysis

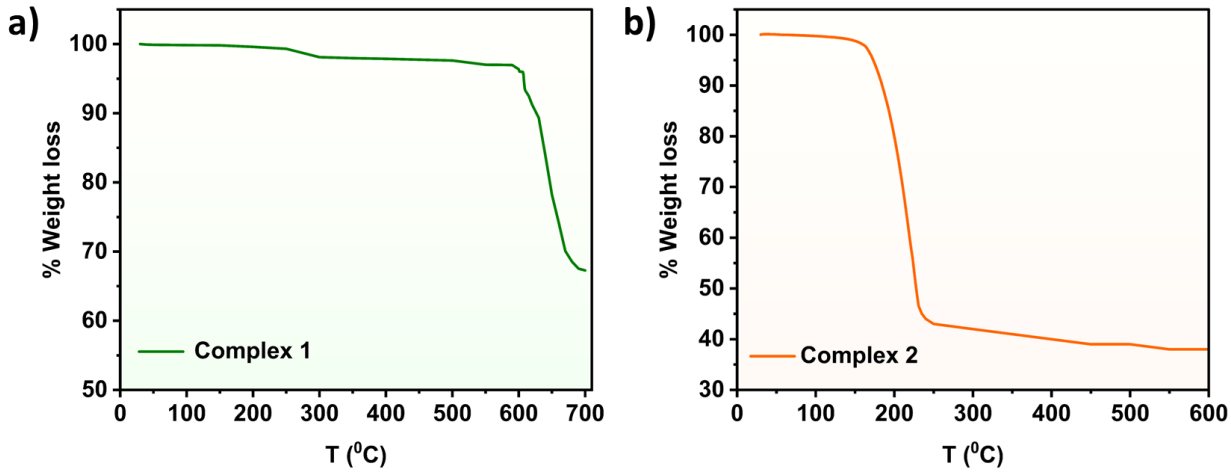

Figure S3: TGA plot of a) complex 1 and b) complex 2.

S5. Hysteresis Measurements

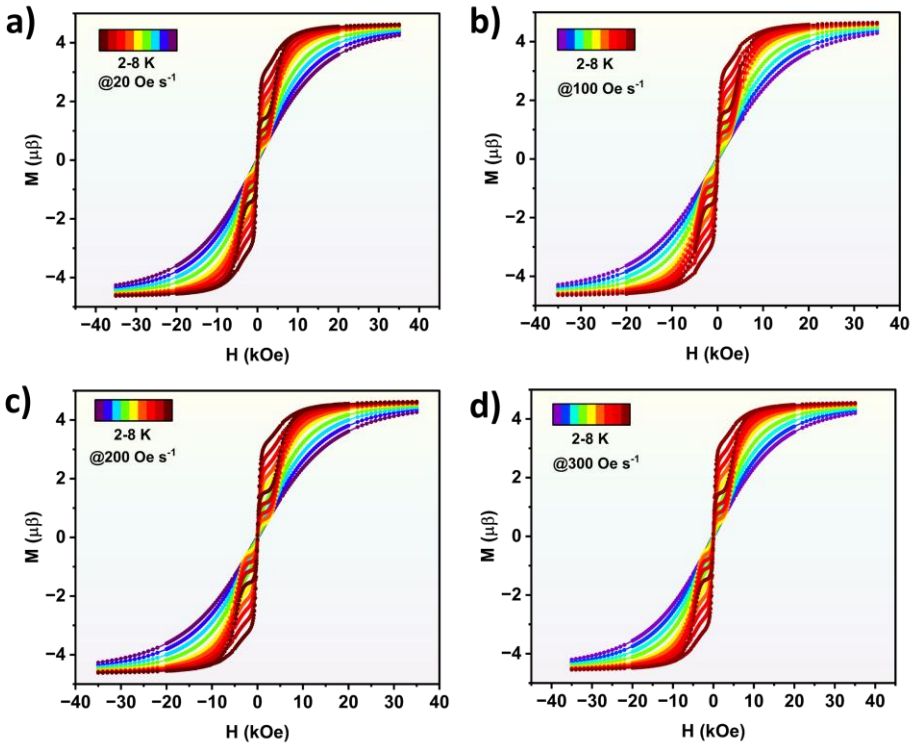

Figure S4: The hysteresis plot of complex 1 in a 2-8 K temperature range at a) 20, b) 100, c) 200 and d) 300 Oe s^{-1}.

S6. Magneto-thermometry Analysis

Extraction of the thermometry parameters from the hysteresis data:

The saturation magnetisation (M_S), remanent magnetisation (M_R), and loop area (A) from magnetic hysteresis data were extracted by following the protocols as mentioned below:

a) **Saturation Magnetisation:** The saturation magnetisation value was taken from the high-field region (|H| ~ 35 kOe), where M approaches a plateau. To minimise noise, an average value of the top 2–3 points at the field extremes was used as M_S.

b) **Remanent Magnetisation:** The remanent magnetisation was determined as the intercept of the magnetisation axis (M at H = 0) obtained during the descending branch of the hysteresis loop (after field reversal). The value was symmetrised by averaging the positive and negative intercepts.

c) **Loop Area:** The hysteresis loop area was calculated using the built-in Polygon Area function in Origin, which integrates the enclosed M–H curve between the forward and backward branches. The area represents the energy dissipated during one magnetisation cycle and was reported in units of μ_β·kOe per molecule (corresponding to magnetisation in μ_β and field in kOe).

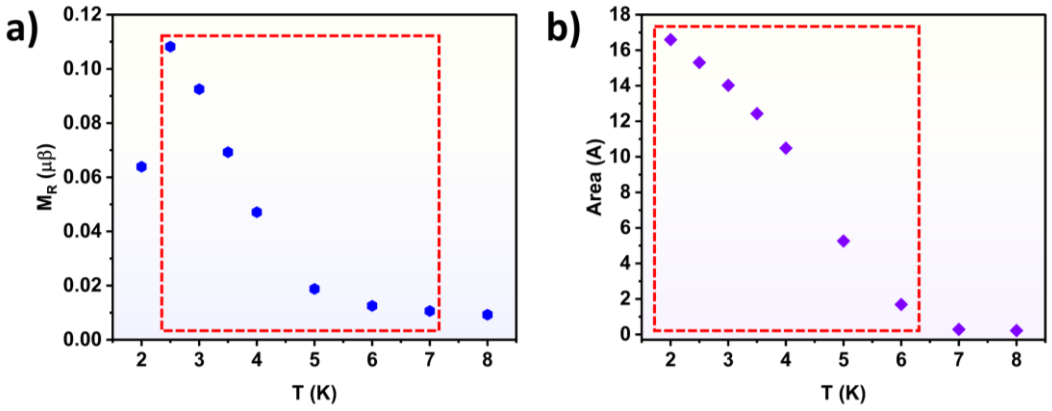

Figure S5. The temperature dependence of the a) remanent magnetisation, and b) area (200 Oe s^{-1}), depicting the region considered for fitting for complex 1. For other scan rates, similar regions have been considered for fitting.

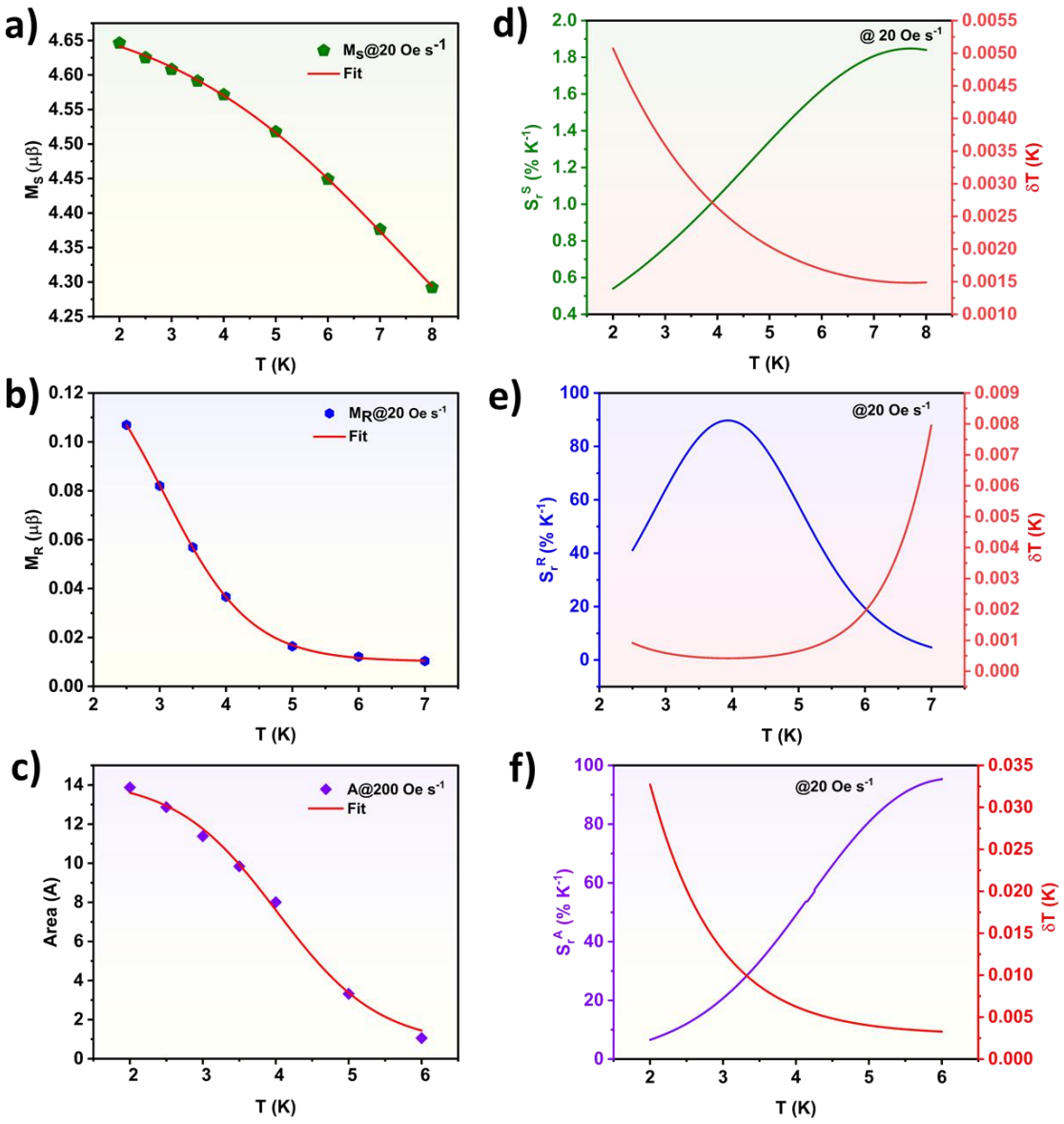

Figure S6. The temperature dependence and corresponding fit of the a) saturation magnetisation, b) remanent magnetisation, and c) area. The relative thermal sensitivity and temperature uncertainty for d) saturation magnetisation, e) remanent magnetisation, and f) area at a scan rate of 20 Oe s^{-1} for complex 1.

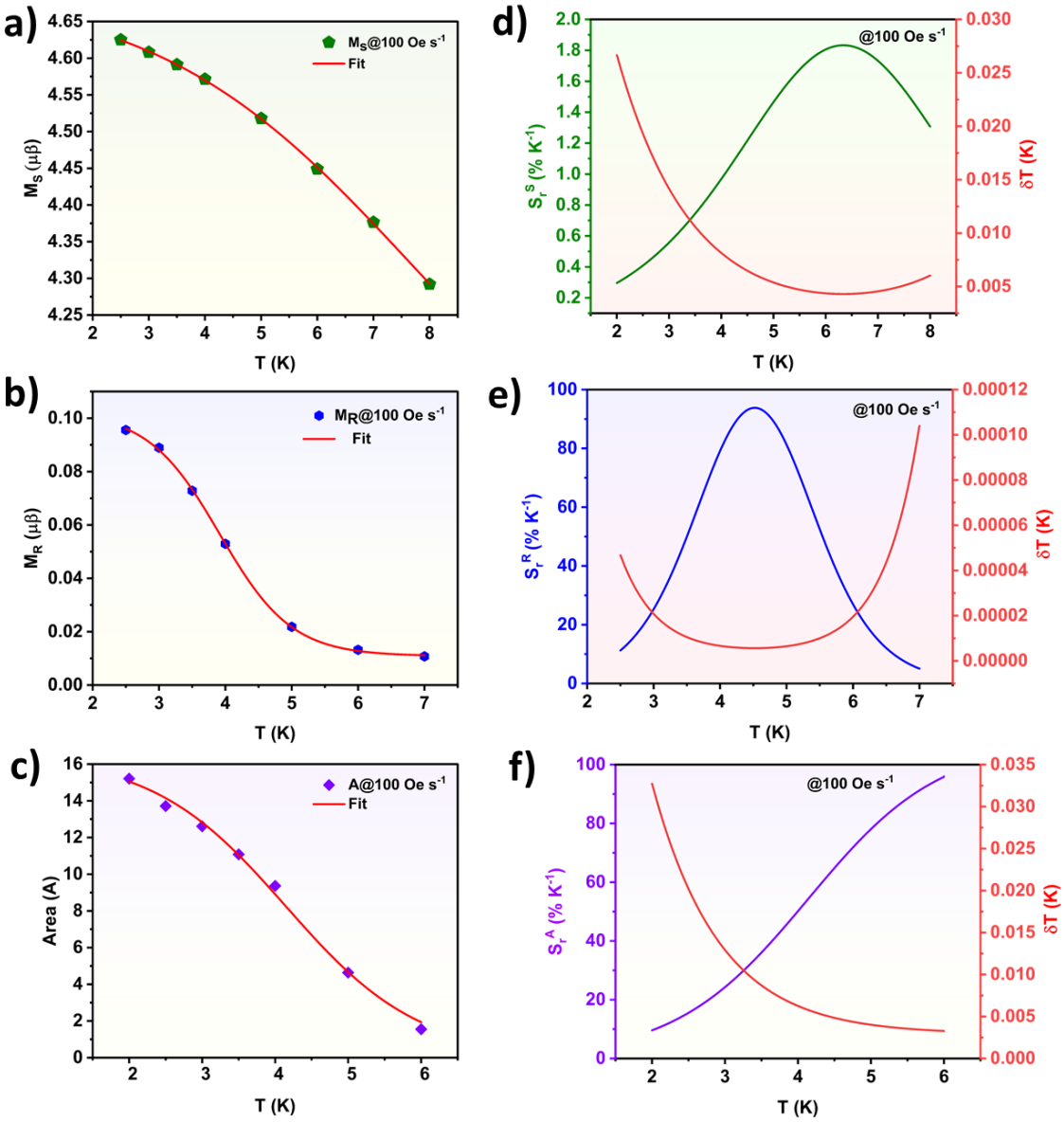

Figure S7. The temperature dependence and corresponding fit of the a) saturation magnetisation, b) remanent magnetisation, and c) area. The relative thermal sensitivity and temperature uncertainty for d) saturation magnetisation, e) remanent magnetisation, and f) area at a scan rate of 100 Oe s^{-1} for complex 1.

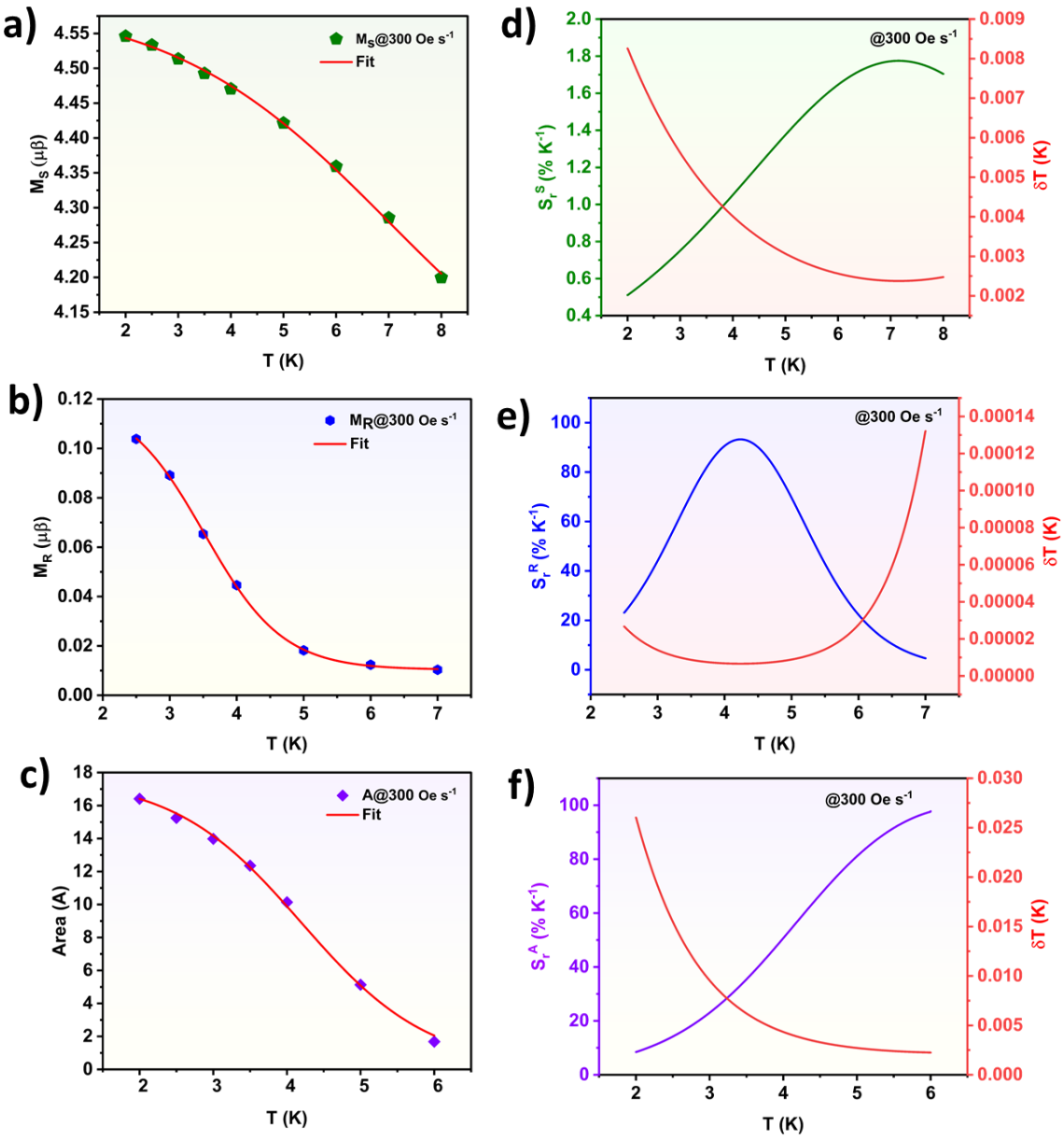

Figure S8. The temperature dependence and corresponding fit of the a) saturation magnetisation, b) remanent magnetisation, and c) area. The relative thermal sensitivity and temperature uncertainty for d) saturation magnetisation, e) remanent magnetisation, and f) area at a scan rate of 300 Oe s^{-1} for complex 1.

Table S1. The fitting parameters of complex 1 for saturation magnetisation-based temperature calibration using equation 1.

Saturation Magnetisation	20 Oe s^{-1}	100 Oe s^{-1}	200 Oe s^{-1}	300 Oe s^{-1}
A_1	4.705 ± 0.006	4.690 ± 0.012	4.666 ± 0.008	4.596 ± 0.012
A_2	3.962 ± 0.005	4.011 ± 0.085	4.035 ± 0.010	3.963 ± 0.013
T_0	7.501 ± 0.028	7.681 ± 0.448	7.002 ± 0.040	7.006 ± 0.036
dT	2.322 ± 0.090	2.287 ± 0.234	1.994 ± 0.096	2.085 ± 0.132

Table S2. The fitting parameters of complex 1 for remanent magnetisation-based temperature calibration using equation 1.

Remanent Magnetisation	20 Oe s^{-1}	100 Oe s^{-1}	200 Oe s^{-1}	300 Oe s^{-1}
A_1	0.147 ± 0.003	0.102 ± 0.001	0.124 ± 0.002	0.120 ± 0.003
A_2	$0.010 \pm 3.395E^{-4}$	$0.011 \pm 6.288E^{-4}$	$0.010 \pm 4.946E^{-4}$	$0.010 \pm 7.076E^{-4}$
T_0	3.065 ± 0.038	3.913 ± 0.023	3.543 ± 0.025	3.517 ± 0.039
dT	0.650 ± 0.018	0.542 ± 0.023	0.589 ± 0.020	0.586 ± 0.031

Table S3. The fitting parameters of complex 1 for area-based temperature calibration using equation 1.

Area	20 Oe s^{-1}	100 Oe s^{-1}	200 Oe s^{-1}	300 Oe s^{-1}
A_1	14.311 ± 0.507	16.512 ± 0.449	17.502 ± 0.449	17.713 ± 0.682
A_2	0.121 ± 0.003	0.132 ± 0.007	0.256 ± 0.010	0.156 ± 0.003
T_0	4.021 ± 0.083	4.145 ± 0.043	4.245 ± 0.037	4.195 ± 0.028
dT	0.697 ± 0.067	0.917 ± 0.041	0.836 ± 0.033	0.866 ± 0.026

Magnetothermometry of $[Dy(L^{N6}_{phen})(Ph_3SiO)_2](PF_6)$ (Complex 2):

To check the applicability of this strategy in other molecules, we have synthesised $[Dy(L^{N6}_{phen})(Ph_3SiO)_2](PF_6)$ (Complex 2) as reported by Armenis *et al*.[3] We have recorded the hysteresis data in the 2.5-5 K range with a scan rate of 50 Oe s^{-1}. The remanent and saturation magnetisation were considered as thermometry parameters (Figure S8). The molecule did not show wide loops, so we could not use the loop area for thermometry measurements. The narrow hysteresis indicates faster magnetic relaxation (high QTM), leading to a very small loop area (~0.216 μ_β·kOe at 2.5 K) that lies within experimental noise. As a result, the temperature dependence of the area could not be resolved reliably, and only M_S and M_R were used for thermometric analysis. Similar to complex 1, the remanent magnetisation yielded better sensitivity compared to the saturation magnetisation in complex 2. This shows that hysteresis-based thermometry can be employed for other classes of SMMs, apart from the discussed complex 1 in the manuscript. For Complex 2, the saturation magnetisation yielded S_{max} of 1.1 % K^{-1} (at 4.3 K) and remanent magnetisation yielded a S_{max} of 31 % K^{-1} (at 3.6 K). For both parameters, the temperature uncertainty was well within an acceptable range (< 0.1 K). For remanent magnetisation, the sensitivity was above 1 % K^{-1} in the entire temperature range of 2.5-5 K. However, the lower S_{max}^R value of Complex 2 (31 % K^{-1}) compared to Complex 1 (96 % K^{-1}) arises from differences in their magnetic anisotropy and relaxation behaviour. Complex 1, with nearly ideal D_5h symmetry, exhibits strong axial crystal-field splitting and suppressed quantum tunnelling of magnetisation ($\tau_{QTM} \sim 0.24$ s)[4], leading to larger remanence and higher thermal sensitivity. In contrast, the pseudo-D_6h symmetry of Complex 2 introduces stronger transverse components that enhance QTM ($\tau_{QTM} \sim 1.6 \times 10^{-2}$ s)[3], resulting in faster relaxation and hence reduced remanent magnetisation and sensitivity.

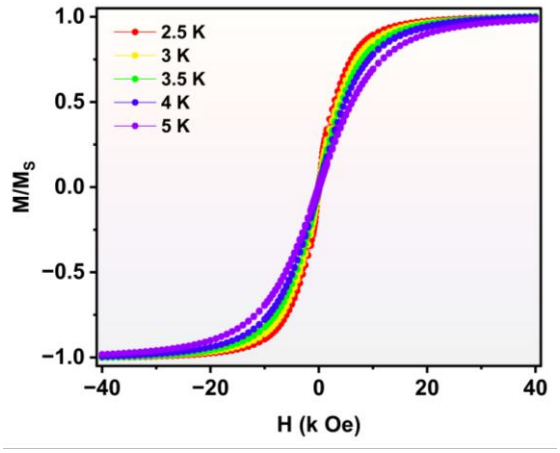

Figure S9. The variable temperature hysteresis data of complex 2 at a scan rate of 50 Oe s^{-1}.

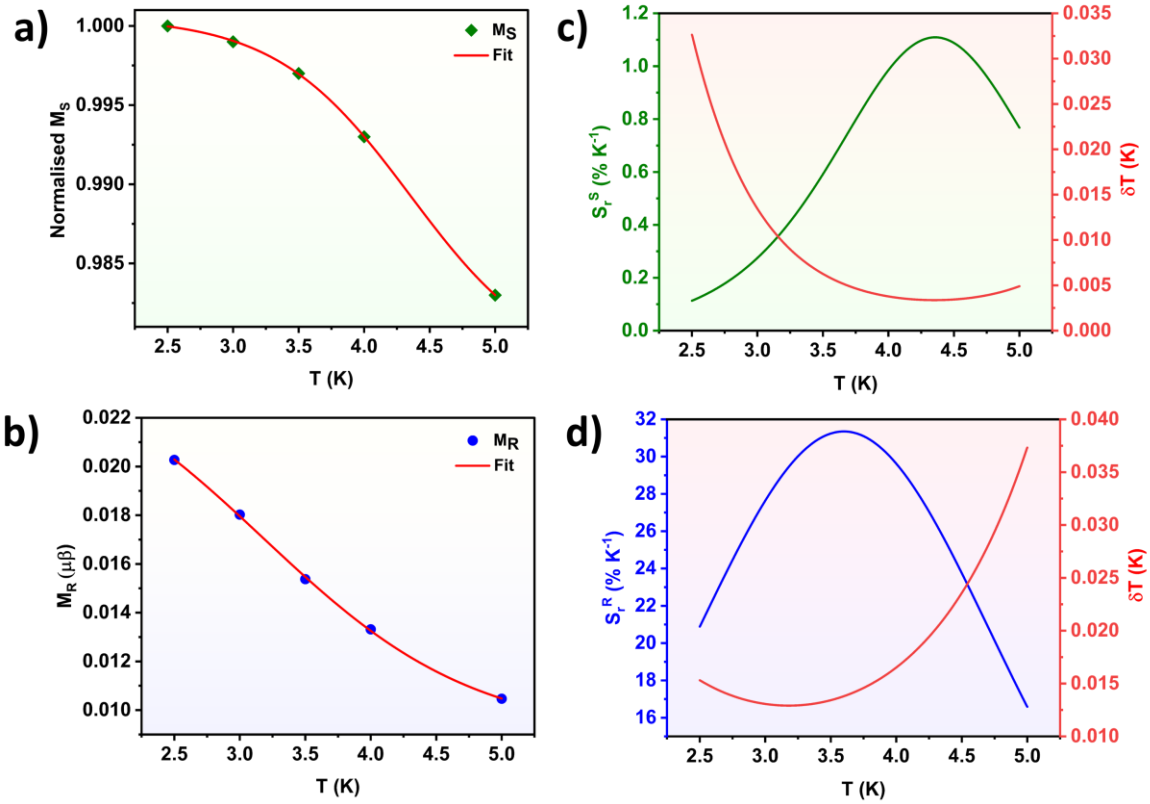

Figure S10. The temperature dependence and corresponding fit of the a) saturation magnetisation, and b) remanent magnetisation, the relative thermal sensitivity and temperature uncertainty for c) saturation magnetisation, and d) remanent magnetisation at a scan rate of 50 Oe s^{-1} for complex 2.

Table S4: The comparison of relative thermal sensitivity for the three thermometry parameters under different scan rates for complex 1.

Thermometry Parameter	Scan Rate (Oe s^{-1})	S_{max} (% K^{-1})	T_{max} (K)	T (K) with S_r > 1 % K^{-1}
Saturation Magnetisation	20	1.9	7.7	3.7-8
	100	1.8	7.7	3.8-8
	200	1.8	7.1	3.9-8
	300	1.8	7.1	3.8-8
Remanent Magnetisation	20	89.7	3.93	2.5-7
	100	93.8	4.5	2.5-7
	200	93.6	4.2	2.5-7
	300	93.2	4.2	2.5-7
Loop Area	20	95.4	6	2-6
	100	95.9	6	2-6
	200	96.4	6	2-6
	300	97.7	6	2-6

Advantages and drawbacks of hysteresis-based thermometry in SMMs:

The present study introduces a proof-of-concept demonstration of magnetic hysteresis-based thermometry in single-molecule magnets (SMMs). The approach utilises the temperature dependence of key magnetic parameters: saturation magnetisation (M_s), remanent magnetisation (M_r), and hysteresis loop area (A), as intrinsic thermal markers in the cryogenic regime (2–8 K). Unlike conventional luminescence thermometry, which depends on optical signal intensity ratios and becomes unreliable below 10 K due to frozen Boltzmann populations, this method directly relies on the intrinsic spin-phonon coupling and magnetic relaxation dynamics governing the SMM behaviour. The parameters M_s, M_r, and A show reproducible and monotonic temperature trends, enabling reliable calibration without the need for optical probes, emissive ligands, or external reference channels. The multiparametric nature of the method further allows internal validation; if one parameter shows limited sensitivity, others (notably loop area) retain strong thermal response and robustness against experimental noise.

From a practical standpoint, we acknowledge that the current implementation relies on a SQUID magnetometer, which already includes precise temperature control. However, this setup serves primarily as a controlled calibration platform to validate the principle. The broader value lies in the transferability of the concept to miniaturised magnetic readouts such as micro-Hall sensors, nanoSQUIDs, or magneto-optical detectors, where direct temperature measurement may be difficult or intrusive. Some instrumental and physical constraints must be acknowledged: (i) hysteresis parameters show mild dependence on field sweep rate, requiring standardized sweep protocols for reliable calibration; (ii) applicability is limited to magnetically robust SMMs that retain open hysteresis at low temperatures; (iii) the method loses sensitivity above the blocking temperature as hysteresis collapses; and (iv) magnetic measurements inherently offer lower temporal resolution than optical techniques. Nevertheless, once calibrated, this intrinsic, magnetically encoded thermometric strategy provides a valuable and conceptually distinct complement to luminescence thermometry, particularly

effective in the sub-10 K regime where optical approaches typically fail. Its integration with on-chip magnetic sensors offers a potentially scalable route toward local and non-contact cryogenic thermometry in quantum and molecular spintronic devices.

Table S5: A comparative table of multifunctional lanthanide SMMs using conventional thermometry approaches, luminescence thermometry, magneto-thermometry, magnetic circular dichroism (MCD), and multiparametric thermometry by MLR. (If not mentioned, the S_{max} values are based on luminescence thermometry)

Formulae	Symmetry	SMM range (K)	U_{eff} (K)	S_{max} (T_{max})	~T range (S_r > 1%K^{-1})	Reference
Luminescence Thermometry						
$[Dy_2(bpm)(tfaa)_6]$	D_{4d}	1.8-11	33	1.8 (5.4) 0.5 (90) 3.3 (298)	5.4-85.5 90-300 298-398	*ACS Cent. Sci.*, **2019**, *5*, 1187−1198
$\{[Ho^{III}(4\text{-pyridone})_4(H_2O)_2][Co(CN)_6]\}\cdot nH_2O$	D_{5h}	2-15	90	6.9 (40)	2-140	*Chem. Sci.*, **2021**, *12*, 730-741
$[Dy(acac)_3(H_2O)_2]$	D_{2d}	4-12	95	5.5 (40) (under 3.6 T)	20-110	*Adv. Optical Mater.*, **2021**, *9*, 2101495
$[Dy(acac)_3(H_2O)_2]$	D_{2d}	4-12	95	5.5 (40) (under 3.6 T)	20-110	*Adv. Optical Mater.*, **2021**, *9*, 2101495
$[Dy_x^{III}Y_{1-x}^{III}(phen)_2(\mu\text{-}OH)_2(H_2O)_2]\cdot[AuI(SCN)_2]_2\cdot phen$	D_{2d}	1.85-4 (Under 500 Oe DC)	91	3.5 (55)	100-300	*Adv. Optical Mater.*, **2022**, *10*, 2201675
$[DyCo(CN)_6(bpyO_2)_2(H_2O)_3]$	D_{2d}	2-10.7 (Under 3000 Oe DC)	86	1.84 (70)	40-140	*Inorg. Chem.*, **2022**, *61*, 5, 2546
$[Dy_4(1,1,4\text{-}H3Lr)_2(OAc)_6]$	D_{2d}/D_{4d}	3-17	40	1.6 (291)	175-300	*Dalton Trans.*, **2022**, *51*, 15593
$\{Tb^{III}[Co^{III}(CN)_6]\}$	D_{3h}	2-42	855	5.28 (16)	6-92	*Angew. Chem. Int. Ed.*, **2023**, *62*, e202306372
$[Dy(acac)_3(bpm)]$	D_{4d}	1.8-24	309	1.51 (70)	30-140	*Chem. Commun.*, **2023**, *59*, 8723
$\{[Dy(L^{N6prop})(OAc)_2](NO_3)\}\cdot CHCl_3$	C_{2v}	4-6.5 (Under 2000 Oe DC)	127	5.1 (286)	200-300	*Inorg. Chem. Front.*, **2024,** *11*, 1087
$[Dy_2(L_{Np})_6(bpym)]$	D_{2d}	2-12	50	1.60 (46)	16-117	*Chem. Commun.*, **2025**, *61*, 2337
Other Optical Thermometry						
$[Ho(acac)_3(phen)]$ Magnetic-circular dichroism, MCD	D_{4d}	-	23	95.3 (2.54 K) from MLR using 0.25 T field	1.55-5	*Angew. Chem. Int. Ed.*, **2023**, *62*, e202309152
$[NdL(CF_3SO_3)_3]$ Luminescence Manometry	-	1.8-3.6 (Under 1000 Oe DC)	23	0.5 (20 K) under 2.85 nm/Gpa	-	*Adv. Optical Mater.*, **2025**, *13*, 2500495
[Dy(acac)3(phen)] Magnetic-circularly polarised luminescence, MCPL	D_{4d}	2-17	63.84	19.7 (293 K) 30.6 (293 K) from MLR	213-293	*Angew. Chem. Int. Ed.*, **2025**, e202505806
Magneto Thermometry						
$[Dy(bbpen)Cl]$	D_{5h}	2-50	943	0.30 (225) from PL 0.06 (225) from $1/\chi$ 0.35 (225) from τ 28 (12) from MLR	- - - 12-300	*Angew. Chem. Int. Ed.*, **2023**, *62*, e202306970
				Using Hysteresis **1.9 (7.7) from M_S** **93.8 (4.5) from M_R** **97.7 (6) from A**	**10-100** **2.64-45** **15-300**	**This work**

S7. References

1. A. Neves, S. M. D. Erthal, I. Vencato, A. S. Ceccato, Y. P. Mascarenhas, O. R. Nascimento, M. Horner and A. A. Batista, *Inorg. Chem.*, 1992, **31**, 4749-4755.
2. J. Liu, Y.-C. Chen, J.-L. Liu, V. Vieru, L. Ungur, J.-H. Jia, L. F. Chibotaru, Y. Lan, W. Wernsdorfer, S. Gao, X.-M. Chen and M.-L. Tong, *J. Am. Chem. Soc.*, 2016, **138**, 5441-5450.
3. A. S. Armenis, A. Mondal, S. R. Giblin, D. I. Alexandropoulos, J. Tang, R. A. Layfield and T. C. Stamatatos, *Inorg. Chem. Front.*, 2025, **12**, 1214-1224.
4. S. Zanella, M. Aragon-Alberti, C. D. S. Brite, F. Salles, L. D. Carlos and J. Long, *Angew. Chem., Int. Ed.*, 2023, **62**, e202306970.